Soft Matter

Dynamic Article Links

Cite this: *Soft Matter*, 2012, **8**, 8107

www.rsc.org/softmatter

PAPER

Finite element simulation of swelling-induced crack healing in gels

Jiaping Zhang,[a] Yonghao An,[a] Kyle Yazzie,[b] Nikhilesh Chawla[ab] and Hanqing Jiang*[a]

Received 21st February 2012, Accepted 3rd April 2012
DOI: 10.1039/c2sm25399b

Finite element simulations have been conducted to study the evolution of stress fields at the crack tip and the crack opening around the crack tip with time for a gel subject to mode I loading. It is found that the stress singularity at the crack tip is eliminated by the swelling of the gel when the solvent is applied at the crack tip. The swelling of the gel also heals the crack tip and the new crack tip generated by swelling does not have a stress singularity. This crack healing process is also verified by experiments and the strain field is measured by digital image correlation. This crack healing mechanism seems to provide a useful means to improve the mechanical integrity of gels and self-healing in general.

Gels are soft materials where the three dimensional polymer network is immersed in a typical liquid environment. The dual attributes of a solid and a liquid, their environmental sensitivities and some other superior properties, such as biocompatibility, biodegradability and non-toxic nature, make the gel a material of choice in nature and in engineering for a variety of applications, from our daily life[1] (*e.g.*, food and contact lenses), sustained drug delivery,[2] tissue engineering scaffolds,[3] and the oil industry.[4,5] Though some recent improvements on strengthening of gels have been made by double-networking,[6] many gels are mechanically fragile.[7] Thus, it is important to understand the fracture behavior of gels.

Recently, the fracture behavior of gels has aroused some interest in the soft materials community. Hui *et al.*[8] have found that unlike hard materials, soft elastomers showed a blunted crack shape. Krishnan *et al.*[9] numerically studied the crack tip field of elastomers in mode I fracture and showed different stress singularities compared with linear elastic materials. Solvent also plays an important role in gel fracture. It affects crack propagation dynamics, as evidenced by Baumberger *et al.*[10] and Seitz *et al.*[11]

This paper studies another aspect of the influence of the solvent on gel fracture. The solvent swells the gel and thus modifies the stress distribution within the gel. Under this circumstance, swelling-induced healing occurs. This paper studies the healing process using finite element simulations and experiments.

The simulation starts from a coupled field theory[12] that couples the deformation of the polymer network and the diffusion of the solvent. Other models are also available.[13,14] The solid-like property of gels makes it feasible to use the commonly used concept in solid mechanics to describe the deformation from one configuration (with position $\boldsymbol{X}$) to another (with position $\boldsymbol{x}(\boldsymbol{X},t)$). By tracking the trajectory of the markers upon deformation, the macroscopic deformation gradient $\boldsymbol{F} = \partial \boldsymbol{x}(\boldsymbol{X},t)/\partial \boldsymbol{X}$ is defined and the stress tensor is work conjugate with deformation gradient $\boldsymbol{F}$, *i.e.*, $\boldsymbol{s} = \partial W(\boldsymbol{F},\mu)/\partial \boldsymbol{F}$. Here $\boldsymbol{s}$ is the nominal stress (force per area in the reference state) and $W(\boldsymbol{F},\mu)$ is the nominal free energy density as a function of deformation gradient $\boldsymbol{F}$ and chemical potential μ. One choice of the free energy density $W(\boldsymbol{F},\mu)$ is the Flory–Huggins model,[15,16] where $W(\boldsymbol{F},\mu)$ is given by

$$\begin{aligned} W(\boldsymbol{F},\mu) = {} & \frac{1}{2}Nk_{\mathrm{B}}T[F_{iK}F_{iK} - 3 - 2\log(\det\boldsymbol{F})] \\ & - \frac{k_{\mathrm{B}}T}{v}\left[(\det\boldsymbol{F} - 1)\log\left(\frac{\det\boldsymbol{F}}{\det\boldsymbol{F} - 1}\right) + \frac{\chi}{\det\boldsymbol{F}}\right] \\ & - \frac{\mu}{v}(\det\boldsymbol{F} - 1) \end{aligned} \tag{1}$$

Here N is the number of polymer chains in the gel divided by the volume of the gel in the reference state; $k_{\mathrm{B}}T$ is temperature in the unit of energy; v is the specific volume of solvent molecule; and χ is a dimensionless parameter characterizing the enthalpy of mixing. Cauchy stress $\boldsymbol{\sigma}$ can be obtained from nominal stress $\boldsymbol{s}$ and expressed as

$$\begin{aligned} \sigma_{ij} = {} & \frac{Nk_{\mathrm{B}}T}{\det(\boldsymbol{F})}F_{iK}F_{jK} + \frac{k_{\mathrm{B}}T}{v}\delta_{ij} \\ & \left[-\frac{Nv}{\det\boldsymbol{F}} - \log\left(\frac{\det\boldsymbol{F}}{\det\boldsymbol{F} - 1}\right) + \frac{1}{\det\boldsymbol{F}} + \frac{\chi}{(\det\boldsymbol{F})^2} - \frac{\mu}{k_{\mathrm{B}}T}\right] \end{aligned} \tag{2}$$

The nominal free energy density $W(\boldsymbol{F},\mu)$ and stress ($\boldsymbol{s}$ and $\boldsymbol{\sigma}$) can be normalized by $k_{\mathrm{B}}T/v$. Thus, two dimensionless parameters, Nv and χ, are introduced, which determine the equilibrium state of the gels. $Nv = 0.001$ and $\chi = 1.13$ are used in most of the simulations in this paper, which gives the equilibrium swelling ratio $\lambda_{\mathrm{eq}} = 1.1$. Here the relatively smaller swelling ratio is used for the sake of easier convergence and less computational efforts.

[a]*Mechanical and Aerospace Engineering, School for Engineering of Matter, Transport and Energy, Arizona State University, Tempe, AZ, 85287, USA. E-mail: Hanqing.Jiang@asu.edu*
[b]*Materials Science and Engineering, School for Engineering of Matter, Transport and Energy, Arizona State University, Tempe, AZ, 85287, USA*

The dynamic behavior (or equivalently, diffusion behavior) of gels follows Fickian law. In large deformation, the flux of solvents $\boldsymbol{J}$ is taken to be linear in the gradient of the chemical potential of the solvent,

$$J_K = -M_{KL}(\boldsymbol{F}, \mu)\frac{\partial \mu(\boldsymbol{X}, \boldsymbol{t})}{\partial X_L} \tag{3}$$

where M_{KL} is the mobility tensor, given by

$$M_{KL} = \frac{D}{k_B T}(\det \boldsymbol{F} - 1)F_{Ki}{}^{-1}F_{Ki}{}^{-1} \tag{4}$$

where D is the diffusivity and $\boldsymbol{F}^{-1}$ is the inverse of deformation gradient $\boldsymbol{F}$. The mobility tensor is symmetric and positive-definite as required by the second law of thermodynamics. The characteristic time scale is given by $L_{rep}{}^2/D$, where L_{rep} is the characteristic length in a boundary value problem. In the following simulation, all lengths are normalized by L_{rep} and the time is normalized by $L_{rep}{}^2/D$.

The methodology of the finite element simulation follows our previous work,[17] except that a separated in-house program is developed to allow further flexibility over a previously used user-defined element subroutine (UEL) in the commercial software package ABAQUS. Part of the simulation is accomplished using a user-defined hyperelastic material (UHYPER) in ABAQUS.[18]

Fig. 1a illustrates the geometry of model. The boundary conditions are fixed support at the rightmost ($u_1(x = L/2) = u_2(x = L/2) = u_3(x = L/2) = 0$) and a prescribed displacement load is applied at $x = -L/2$ and $y = \pm W$, *i.e.*, $u_2(x = -L/2, y = W) = u_0$ and $u_2(x = -L/2, y = -W) = -u_0$. In order to study the stress and displacement fields at the crack tip before and after the solvent is applied, a two-step process is used. In the first step, a dry gel (*i.e.*, chemical potential $\mu = -\infty$) is subjected to a displacement load $\pm u_0$ at $x = -L/2$ and $y = \pm W$, respectively. Then a droplet of solvent (chemical potential $\mu = 0$) is applied at the crack tip ($x = y = 0$) while the prescribed displacement remains at $x = -L/2$ and $y = \pm W$. Thus, in the second step, the fields of displacement of chemical potential of the gel will evolve. The displacement u_3 is set to be zero.

The symmetry of the model is utilized and Fig. 1b shows a representative mesh that contains 3861 three-dimensional brick elements. The symmetric boundary conditions are applied at $Y = 0$ and $X > 0$ and the crack faces are traction free. This model is considered as the global model. We take a circular domain of radius R centered at the crack tip as our submodel (Fig. 1c) to obtain a finer resolution at the crack tip. The submodel is subjected to a prescribed displacement boundary condition provided by the global model. In the following simulation, we take $L = 80$ and $W = 20$ and the size of the submodel R is 1.25×10^{-2}. The submodel zone contains 28 950 three-dimensional brick elements. A very fine mesh is used near the crack tip. Thus, the largest element size is approximately 2.0 (Fig. 1b) and the smallest element size is 1.3×10^{-5} (Fig. 1c), which provides a ratio of 10^5 between the largest element size to smallest element size. Efforts are made to ensure that elements have an aspect ratio close to 1. Mesh refinement and comparison of different meshes have ensured that the numerical results are accurate.

Fig. 2 shows the normalized vertical stress ($\sigma_{yy}/(k_B T/v)$) of the dry gel *versus* the normalized distance to the crack tip X, ahead of

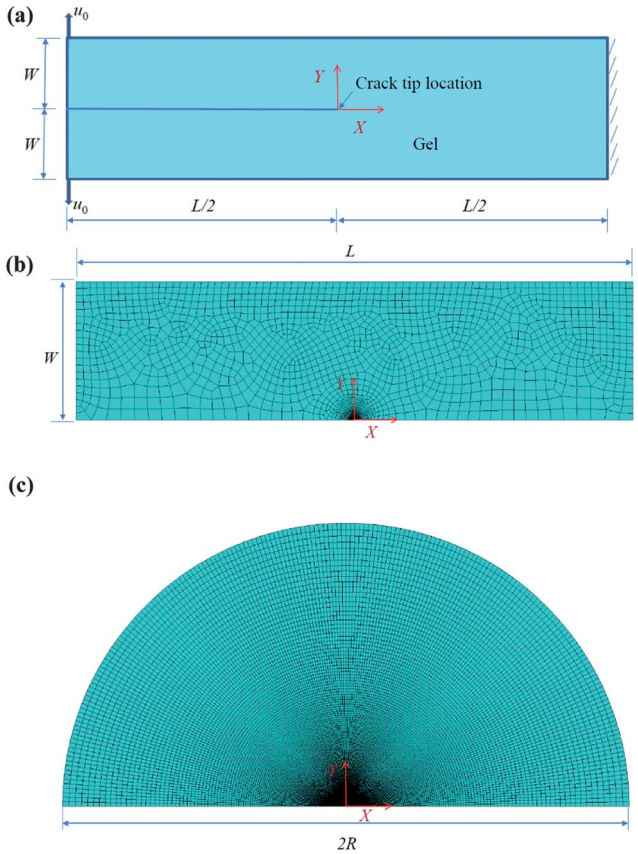

Fig. 1 (a) A gel model with a rectangle geometry $2W \times L$ used in the analysis. The crack tip is located at the center and the crack surface extends to the left. The rightmost of the gel is clamped. Prescribed displacements u_0 are applied at the upper and lower left corners of the model. (b) Finite element mesh for half of the model with a rectangle geometry $W \times L$. The symmetric boundary conditions are applied at $Y = 0$ and $X > 0$. The crack faces are traction free. This model is considered as a global model. (c) Finite element mesh for the submodel near the crack tip. The center of the circle is the crack tip. The radius of the submodel is R.

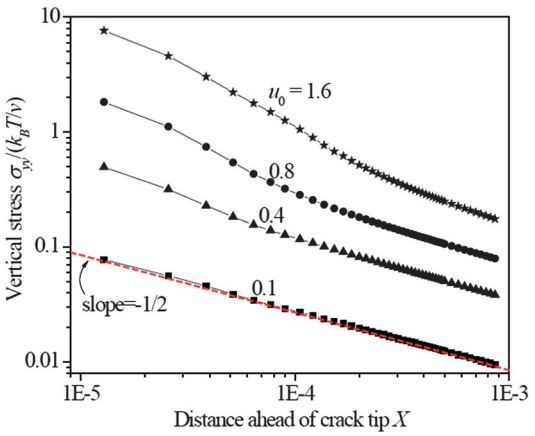

Fig. 2 The distribution of normalized vertical stress $\sigma_{yy}/(k_B T/v)$ ahead of the crack tip for dry gel subjected to different loading $u_0 = 0.1$, 0.4, 0.8 and 1.6. Dashed line is a straight line bearing slope $-1/2$, indicating the square root singularity.

the crack tip during the first step for four sets of prescribed load, $u_0 = 0.1$, 0.4, 0.8, and 1.6. It is observed that for smaller loading (*e.g.*, $u_0 = 0.1$), the stress profile follows a straight line with slope $-1/2$ near the crack tip, this is known as square-root singularity in linear elastic fracture mechanics stating that stress varies as $-1/2$ order of the distance from the crack tip. As the load increases, the stress around the crack tip ($X < 1 \times 10^{-4}$) is evaluated and shows a stronger singularity compared with linear elasticity. This stronger singularity has been attributed to the effect of hyperelasticity.[8,9] Away from the crack tip, the stress still shows $-1/2$ singularity and a transition exists. The following simulations use $u_0 = 0.1$ for the sake of computational simplicity, though similar results have been found for large prescribed displacement (*e.g.*, $u_0 = 0.4$).

The solvent is then dropped at the crack tip in the second step. The wetting process is simulated using the submodel mesh. The nodes on the outer half circle are subjected to the displacement field obtained from the global mesh and the symmetric boundary conditions are applied along the crack extension. Since the solvent will swell the elements, stiff spring elements are employed to prevent element penetration through the symmetric axis ($Y = 0$). Thus, in the second step, some regions of the crack faces do not have traction free boundary conditions depending on the swelling of the gel.

Fig. 3a–c show the stress contours near the crack tip at different times after the solvent droplet is applied at the crack tip. In order to have a fair comparison, the same scale bar is used in all the contours. Since the submodel is used in this simulation, the radius of the submodel R is chosen as the representative length. As shown in Fig. 3a at $Dt/R^2 = 0.31$, the tensile stress still dominates the stress field at the crack tip, though the stress level is a little bit diminished because of the swelling of the crack tip. At $Dt/R^2 = 1.53$ as shown in Fig. 3b, the tensile stress has been further reduced and the stress at the original crack tip turns to compressive. The stress singularity at the crack tip disappears. It is also interesting to notice that since the swelling of the crack tip, the crack is healed, as the new crack tip ($X = -1.293 \times 10^{-4}$) is generated to the left of the original crack tip. Since the new crack tip is generated by the swelling of the gel but not the tensile load, the stress singularity does not exist at the new crack tip. The swelling induced healing in some polymers has been observed.[19] Fig. 3c shows that as time evolves, at $Dt/R^2 = 2.15$, the crack continues to close and the new crack tip has travelled to $X = -0.00163$. The compressive stress at the original crack tip increases and creates a compressive zone near the original crack tip. In the present analysis, the influence of the submodel to the global model is assumed to be insignificant so that the time is limited to a point at which the swelling is still localized near the crack tip and does not affect the global model. The entire crack closure process is still foreseen based on the trends shown in Fig. 3b and c.

The localized swelling at the crack tip results in a tensile to compressive stress transition and crack closure. After very short time since the solvent is applied at the crack tip, the crack tip does not have time to swell such that the tensile stress still dominates (Fig. 3a). As swelling progresses, material near to the crack tip absorbs a large amount of solvent and generates an inhomogeneous swelling field. Swelling at the crack tip releases the tensile stress and even turns it to a compressive stress as the swollen

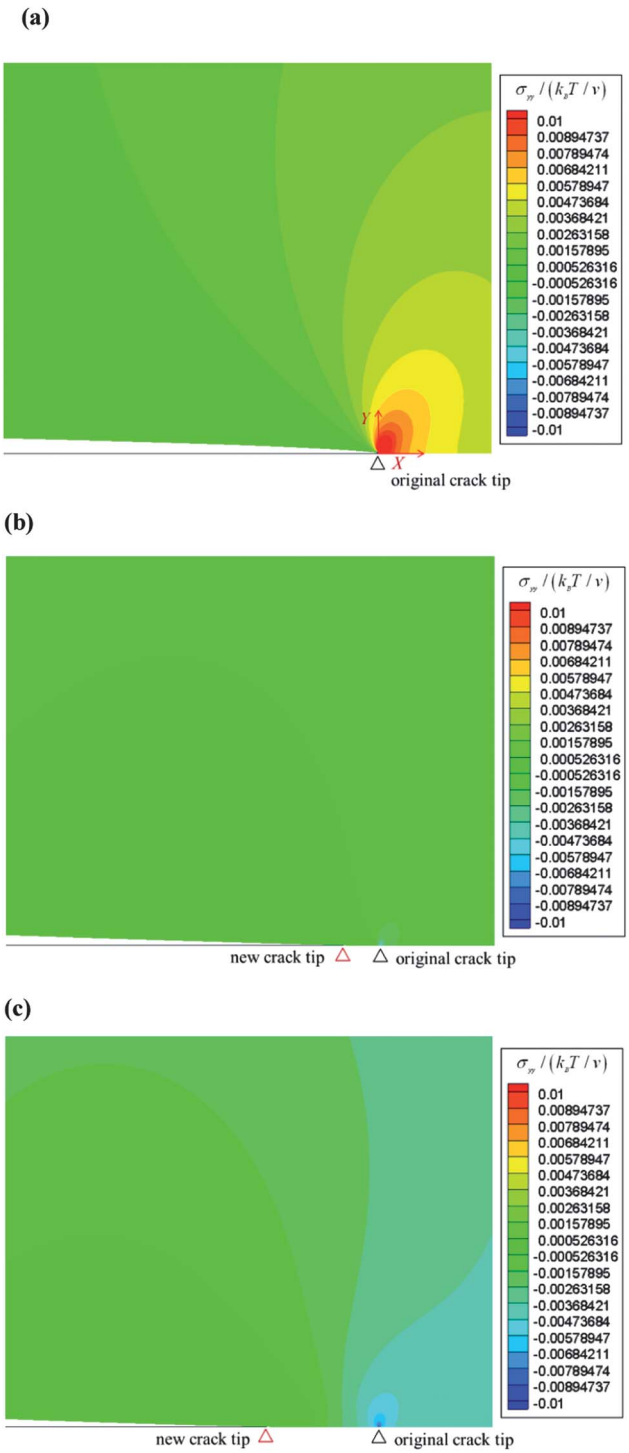

Fig. 3 Contour of the normalized vertical stress $\sigma_{yy}/(k_BT/v)$ around the crack tip at different times after the solvent droplet is applied at the original crack tip at time $t = 0$. (a) $Dt/R^2 = 0.31$ in which the tensile stress at the original crack tip is reduced and the location of the crack tip does not change; (b) $Dt/R^2 = 1.53$ in which the compressive stress appears at the original crack tip and the location of the crack tip changes; (c) $Dt/R^2 = 2.15$ in which a compressive zone appears around the original crack tip and the location of the crack tip moves further. Here R is the radius of the submodel.

elements push each other (Fig. 3b). This process repeats and generates a compressive zone near the original crack tip, as shown in Fig. 3c.

The evolution of stress at the original crack tip and the position of the new crack tip with time are also studied and shown in Fig. 4a. It is found that it only takes a short time to release the tensile stress at the original crack tip and change it to compressive stress. This suggests that even a small amount of solvent present at the crack tip will help to eliminate the stress singularity at the crack tip. Once the stress at the original crack tip turns to compressive, the crack starts to close. It is also observed that once the crack closure is initiated, the location of the new crack tip evolves approximately linearly with time. In other words, a constant crack healing speed occurs in the present analysis. The same constant healing speed is also observed in experiment when poly(methyl methacrylate) swelled in co-solvent of methanol and ethanol.[20]

The constant crack closure speed can be explained by the crack opening u_y at different time Dt/R^2 shown in Fig. 4b. The crack opening u_y at $Dt/R^2 = 0$ corresponds to the case of the dry gel. It is observed that the crack opening profile significantly changes at

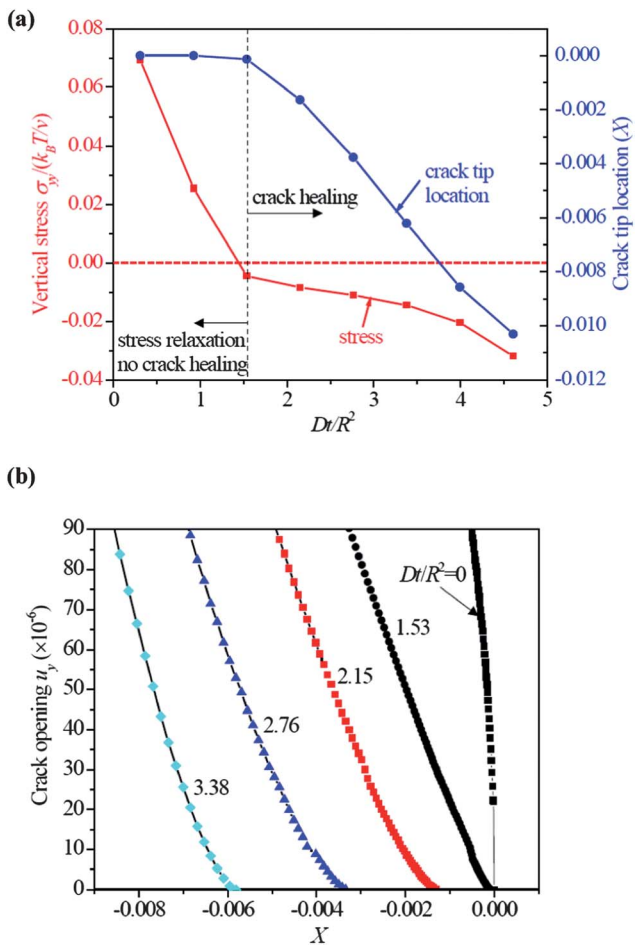

Fig. 4 (a) The normalized vertical stress $\sigma_{yy}/(k_BT/v)$ at the original crack and the location of the crack tip *versus* the normalized time Dt/R^2. (b) Crack opening profile $u_y(X)$ at different time Dt/R^2. $Dt/R^2 = 0$ represents dry gel.

the onset of crack healing (time $Dt/R^2 = 1.53$). Once the crack healing starts, for equal time interval ($Dt/R^2 = 0.62$), the crack opening profiles are self-similar with approximately equal separation in X. Thus, the crack healing is propagating with a constant speed in a similar manner as that of the stress wave.

Despite the fact that the involvement of the solvent decreases the fracture toughness of the gel as shown in Baumberger *et al.*'s experiment,[10] the swelling of the gel compensates this decrease and still leads to crack closure as shown in the simulation and to be shown in the following experiments.

The solvent aided self-healing process of the gel was validated by experiments as well. A poly(ethylene glycol) diacrylate (PEGDA) gel slab with 15 mm in length and 10 mm in width was prepared. The gel was prepared with the solution containing a 1 : 1 (by weight) mixture of cross-linker of PEGDA and polyethylene glycol (PEG), together with 2 wt% photoinitiator, Irgacure 819. The solution was put in a Petri dish and exposed to ultraviolet light with a wavelength of 365 nm. Both sides were exposed for 15 seconds to ensure uniform crosslinking. Equilibrium swelling ratio of the gel was measured to be 1.3. The square, dry, PEGDA gel stab is cut by a razor blade to create a crack, followed by 0.4 mm displacement loading as illustrated in Fig. 1a. A drop of water was then dropped in the crack tip. Then the digital image correlation (DIC) technique was used to measure the displacement and to calculate the strain field. DIC uses a correlation algorithm to compare successive images of a deforming speckle pattern. The speckle pattern is applied to the sample surface, and provides a high contrast pattern that can be easily correlated by the DIC algorithm. The algorithm computes a displacement field based on local correlation of the positions of individual speckles. The speckle pattern was applied to the gel specimen surface as follows. The gel surface was coated with a thin layer of white matte-finish spray paint. Black matte-finish spray paint was sprayed on the white base coat to create a stochastic pattern of speckles on the order of 200 μm width, or about 4 pixels by 4 pixels in area. The test was recorded by taking 8-bit tiff images. The strain produced in the specimen during the tensile test was analyzed by importing the 8-bit tiffs into commercially available digital image correlation software (ARAMIS, Trillion Quality System, Plymouth Meeting, PA, USA).

Fig. 5 shows the strain field at different times after the water droplet is applied at the crack tip. At $t = 0$ (Fig. 5a), *i.e.*, the prescribed displacement load is just applied, and a high tensile strain field is observed around the crack tip. One minute after the water droplet is applied at the crack tip (Fig. 5b), part of the original crack has been closed and the strain field around the original crack tip is reduced. Ten minutes later (Fig. 5c), most of the crack has been closed due to swelling. Thirty minutes later (Fig. 5d), the healing process is complete and the strain field is tremendously reduced.

We also study the effect of the equilibrium swelling ratio of a gel on the crack healing. Thus the static simulations are conducted here. In order to include the effects of the submodel on the global model to study the entire crack closure, the global model is subjected to a uniform chemical potential $\mu = 0$ and the obtained displacement fields are applied to the submodel as the prescribed displacement boundary conditions. Then the crack closure is studied for both the global model and submodel. Gels with

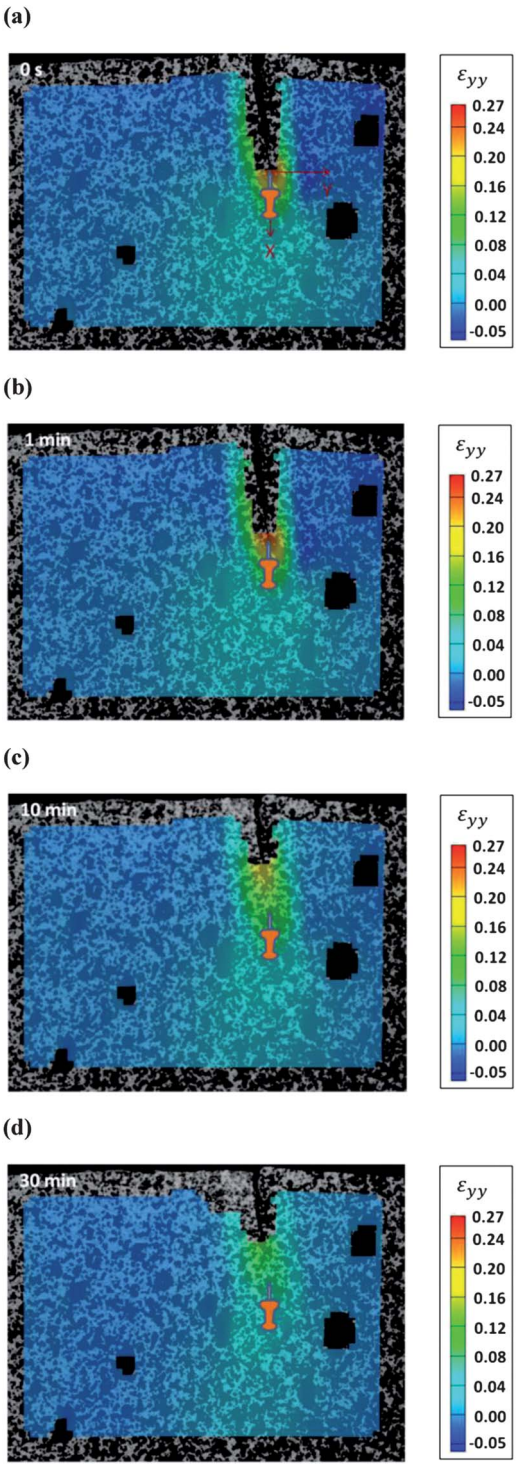

Fig. 5 Strain field obtained by digital image correlation. (a) Strain field right after the square gel slab is subjected to a displacement loading $u_0 =$ 0.4 mm based on Fig. 1a. (b) Strain field of 1 minute after adding solvent. (c) Strain field of 10 minutes after adding solvent. (d) Strain field of 30 minutes after adding solvent.

different equilibrium swelling ratio have been used and the relative crack healing (healed length *versus* submodel size) is plotted as a function of equilibrium swelling ratio in Fig. 6. It can be observed that a very small swelling ratio is insufficient to heal

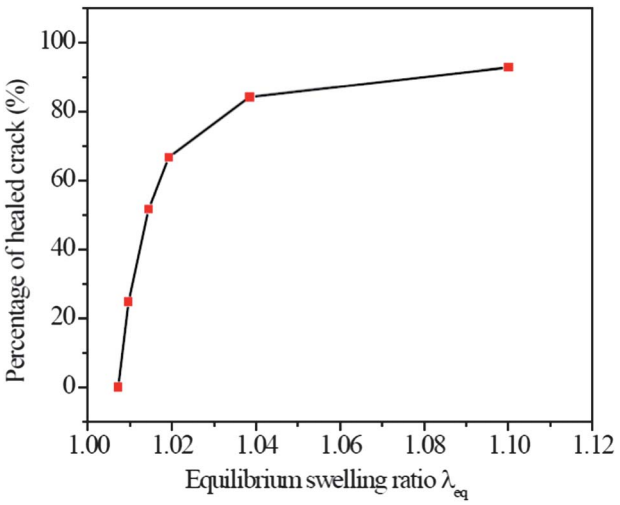

Fig. 6 Percentage of healed crack *versus* equilibrium swelling ratio λ_{eq} of a gel.

the crack. As the equilibrium swelling ratio increases, the percentage of the healing increased drastically. When the equilibrium swelling ratio is 1.1 (*i.e.*, the equilibrium swelling ratio used in the previous analysis), most of the crack has been healed. This result suggests that for a given crack, a corresponding equilibrium swelling ratio exists to ensure that the crack can be healed completely by gel swelling. The equilibrium swelling ratio depends on the polymer crosslink density, the polymer–solvent affinity, and the ambient humidity as well.

In summary, this study shows that the presence of a solvent at the crack tip swells the gel and releases the tensile stress around the crack tip. Crack closure occurs due to gel swelling and the fraction of crack healing depends on the equilibrium swelling ratio of a gel. Future work on the solvent involved gel fracture, such as the evolution of stress field at the crack tip as solvent diffuses using the asymptotic analysis, would be of interest. This work also sheds some light on the practical application of self-healing, though the actual healing process is a much more complicated one that involves polymerization of the healing agent assisted by a catalyst.[21] However, one critical step in healing is to bring the cracked faces in contact[22,23] and the present analysis provides a means to analyze this problem. Once the crack faces come into contact, subsequent healing steps may involve molecular interdiffusion[24] or reversible bonding[25] such as ionic bonding and hydrogen bonding. Moreover, swelling-induced self-healing may provide an alternative way for heat[26] or light[27] based healing. In this spirit, healing by solvent swelling is a promising way to improve the structural integrity of gels, to extend product lifetime, and to broaden their applications.

The authors thank Professor Subramaniam D. Rajan and Dr Gil Speyer in Arizona State University for their useful suggestions in developing the numerical code. We also appreciate the Fulton High Performance Computing at Arizona State University for their support of our simulations.

Notes and references

1 W. Pilnik and F. M. Rombouts, *Carbohydr. Res.*, 1985, **142**, 93–105.
2 Y. Qiu and K. Park, *Adv. Drug Delivery Rev.*, 2001, **53**, 321–339.

3 J. L. Drury and D. J. Mooney, *Biomaterials*, 2003, **24**, 4337–4351.
4 J. A. Gomez, D. D. Mamora and L. O. Lilledal, *SPE Drill. Completion*, 2002, **17**, 82–86.
5 M. Kleverlaan, R. H. van Noort and I. Jones, SPE/IADC Conference, Amsterdam, Netherlands, 2005.
6 J. P. Gong, Y. Katsuyama, T. Kurokawa and Y. Osada, *Adv. Mater.*, 2003, **15**, 1155.
7 I. Levental, P. C. Georges and P. A. Janmey, *Soft Matter*, 2007, **3**, 299–306.
8 C. Y. Hui, A. Jagota, S. J. Bennison and J. D. Londono, *Proc. R. Soc. London, Ser. A*, 2003, **459**, 1489–1516.
9 V. R. Krishnan, C. Y. Hui and R. Long, *Langmuir*, 2008, **24**, 14245–14253.
10 T. Baumberger, C. Caroli and D. Martina, *Nat. Mater.*, 2006, **5**, 552–555.
11 M. E. Seitz, D. Martina, T. Baumberger, V. R. Krishnan, C. Y. Hui and K. R. Shull, *Soft Matter*, 2009, **5**, 447–456.
12 W. Hong, X. H. Zhao, J. X. Zhou and Z. G. Suo, *J. Mech. Phys. Solids*, 2008, **56**, 1779–1793.
13 T. Tanaka and D. J. Fillmore, *J. Chem. Phys.*, 1979, **70**, 1214–1218.
14 M. Doi, *J. Phys. Soc. Jpn.*, 2009, **78**, 052001-1–052001-19.
15 P. J. Flory, *J. Chem. Phys.*, 1941, **9**, 660–661.
16 M. L. Huggins, *J. Chem. Phys.*, 1941, **9**, 440.
17 J. P. Zhang, X. H. Zhao, Z. G. Suo and H. Q. Jiang, *J. Appl. Phys.*, 2009, **105**, 093522-1–093522-9.
18 W. Hong, Z. S. Liu and Z. G. Suo, *Int. J. Solids Struct.*, 2009, **46**, 3282–3289.
19 K. S. Toohey, N. R. Sottos, J. A. Lewis, J. S. Moore and S. R. White, *Nat. Mater.*, 2007, **6**, 581–585.
20 H. C. Hsieh, T. J. Yang and S. Lee, *Polymer*, 2001, **42**, 1227–1241.
21 S. R. White, N. R. Sottos, P. H. Geubelle, J. S. Moore, M. R. Kessler, S. R. Sriram, E. N. Brown and S. Viswanathan, *Nature*, 2001, **409**, 794–797.
22 R. P. Wool, *Soft Matter*, 2008, **4**, 400–418.
23 Q. Wang, J. L. Mynar, M. Yoshida, E. Lee, M. Lee, K. Okuro, K. Kinbara and T. Aida, *Nature*, 2010, **463**, 339–343.
24 R. P. Wool and K. M. Oconnor, *Polym. Eng. Sci.*, 1981, **21**, 970–977.
25 D. Y. Wu, S. Meure and D. Solomon, *Prog. Polym. Sci.*, 2008, **33**, 479–522.
26 X. X. Chen, M. A. Dam, K. Ono, A. Mal, H. B. Shen, S. R. Nutt, K. Sheran and F. Wudl, *Science*, 2002, **295**, 1698–1702.
27 M. Burnworth, L. M. Tang, J. R. Kumpfer, A. J. Duncan, F. L. Beyer, G. L. Fiore, S. J. Rowan and C. Weder, *Nature*, 2011, **472**, 334–337.

